Biochimica et Biophysica Acta 1813 (2011) 850–857

Contents lists available at ScienceDirect

Biochimica et Biophysica Acta

journal homepage: www.elsevier.com/locate/bbamcr

Investigation of the Bcl-2 multimerisation process: Structural and functional implications

Alessia Camperchioli [a,1], Marisa Mariani [a,1], Silvia Bartollino [a,1], Lella Petrella [a,1], Marco Persico [b,2], Nausicaa Orteca [b,2], Giovanni Scambia [a,3], Shohreh Shahabi [c,3], Cristiano Ferlini [a,b,c,4], Caterina Fattorusso [b,*,5,6]

[a] Laboratory of Molecular Oncology, University of the Sacred Hearth, Largo A. Gemelli 1, 86100 Campobasso, Italy
[b] Laboratory of Computational Chemistry, Department of Natural Products Chemistry, Faculty of Pharmacy, University of Naples "Federico II," Via D. Montesano 49, 80131 Napoli, Italy
[c] Danbury Hospital Research Institute, 131 West Street, Danbury, CT 06810, USA

ARTICLE INFO

Article history:
Received 18 October 2010
Received in revised form 15 January 2011
Accepted 7 February 2011
Available online 12 February 2011

Keywords:
Bcl-2 structure/function
Multimeric protein complexes
Apoptosis

ABSTRACT

Bcl-2 plays a prominent role in regulating the function of mitochondria during respiration and in determining the threshold of apoptotic sensitivity. Despite its relevance, the mechanism through which these processes are achieved is still unknown. Using surface plasmon resonance technology to monitor Bcl-2 multimerisation we discovered that a simple dimeric model does not fit with experimental data. A molecular model of the experimentally observed Bcl-2 homomeric complex has been developed. Accordingly, using a panel of mutants we identified in the loop a critical region for the process of Bcl-2 multimerisation. Our results indicate that the Bcl-2 loop posttranscriptional changes can modulate its ability to make homo and hetero-complexes, ultimately leading to functional modulation, suggesting an intriguing relationship between the ability of Bcl-2 to form multimeric complexes and its multi-functional role as a membrane channel.

1. Introduction

Apoptosis functions physiologically to eliminate cells without activating inflammatory processes. Through the apoptotic pathway, normal tissue homeostasis is achieved, including the removal of damaged and infected cells. Disruption of the normal apoptotic process underlies several diseases, most notably cancer, where the imbalance between cell growth and apoptotic rate is responsible for tumor development and metastasis. Chemotherapeutics and physical treatments attempt to reactivate the apoptotic process in cancer cells, with the goal of complete surgical resection of the tumor and metastases or, if surgery is not sufficient, to eradicate the whole disease.

Due to its status as a fundamental homeostatic process in the life cycle of cells, apoptosis is a highly regulated pathway, with a complex network of functions governing control and activation. In this context, the Bcl-2 family occupies a central role, with over 25 Bcl-2 family members identified in mammalian cells to date [1,2]. Sequence homology analysis within the family allowed identification of 4 domains (Bcl-2 homology, BH1–4) [1]. The traditional classification of the Bcl-2 family divides the members into pro-apoptotic and anti-apoptotic proteins. All the pro-apoptotic members possess the BH3 domain and lack the BH4 domain. Some members such as Bad, Bid, and Bim possess only the BH3 domain, which for this reason is defined as the death domain [3]. In contrast the most important anti-apoptotic proteins (Bcl-2, Bcl-XL, Bcl-w, Mcl-1, and A1) possess 4 BH domains. However, this Manichaean divide between death inducers and protectors against death seems false. In point of fact, anti-apoptotic members still possess the BH3 domain, and in some cases they are still able to induce cell death [4–9]. Questions remain about whether the role of these proteins is confined to the regulation of apoptosis or whether they perform other, as yet not fully recognized functions. Some possible candidates for these are suggested by the example of mitochondria, which have long been established as the major site of ATP production through the processes of electron transport and oxidative phosphorylation. The extrusion of protons from mitochondria results in modulation of the chemical environment, including variations in pH and generation

* Corresponding author. Tel.: +39 081678544; fax: +39 081678552.
E-mail address: cfattoru@unina.it (C. Fattorusso).

[1] Were responsible for performing all the experiments of the in vitro part of this work, including preparation of the constructs and recombinant proteins.
[2] Were responsible to perform calculations required for the computational modeling.
[3] Were involved in the experimental design and in the interpretation of the experimental results.
[4] Directed the study for the in vitro section and wrote the first draft of the manuscript.
[5] Directed the molecular modeling study and edited the final version of this manuscript.
[6] These authors contributed equally to this work.

0167-4889/$ – see front matter © 2011 Elsevier B.V. All rights reserved.
doi:10.1016/j.bbamcr.2011.02.006

of a mitochondrial membrane potential (Δψm), which is directly correlated with the intensity of the electron transport effect that is in turn regulated by the availability of ADP as a substrate for F1F0-ATPase. In short, when cells need energy (ATP), ADP increases and mitochondrial production of energy is stimulated. During this process, electron transport also generates reactive oxygen species and oxidative stress. In this context, members of the Bcl-2 protein family play a pivotal role in the sensitization of mitochondrial membranes to ROS [10] and in the production of ROS itself [11], as well as in the regulation of mitochondrial permeability to ATP [12] and, consequently, to Δψm. These latter effects in particular could depend on the fact that Bcl-2 proteins are structurally related to bacterial colicins [13] and are able to form pores in cell membranes. The channel properties of the Bcl-2 protein family members could regulate the entry of K+, Ca++, as well as entry of the critical ADP/ATP, thereby constituting the key regulators not only of apoptosis but also of the mitochondrial function. Paradoxically, Bcl-2 plays an inhibitory function when bound to the voltage-dependent anion channel (VDAC), a macromolecular complex that crosses mitochondrial membranes and is known to play a critical role in the apoptotic process. These intricate functions require interactions with other proteins in the same family as well as posttranscriptional regulators capable of modulating such interactions. Despite its important physiological role, structural studies of Bcl-2 have been hampered by the unavailability of a technology capable of monitoring the formation of such complexes. In this present study we have tried to characterize these processes at the molecular level using surface plasmon resonance technology and we have attempted to produce molecular models of the resulting complexes. Our results indicate that the Bcl-2 loop plays a pivotal role, and that posttranscriptional changes at these level can modulate the ability to make homo and hetero-complexes, ultimately leading to functional modulation.

2. Materials and methods

2.1. Preparation of purified proteins

Human full-length Bcl-2 was obtained from lymphocytes by PCR with PFU Taq-polymerase (Promega) and cloned into pUSE (Upstate Biotechnology). A construct (pUSE-Bcl2Δ) was made in which 49 aa (32–80) were deleted by inverse PCR and replaced with a linker of 4 alanines. The PCR product was then isolated after the BamH1 and EcoRI digestion and subsequently cloned into pQE1 (Qiagen). pQE1-Bcl2 wild type was used as a template to replace serine 70 with alanine (Bcl-2S70A) and glutamic acid (Bcl-2S70E). The mutations were introduced by site directed, ligase-independent mutagenesis (SLIM) in a multiplex PCR reaction. Two tailed primers (forward and reverse) and two no-tailed primers (forward and reverse) to each Bcl-2 mutation were used for each reaction. Purified proteins were freshly purified using AKTA system (GE Healthcare) and Histraps columns (GE Healthcare). Purity was over than 95% and a representative Coomassie gel staining is shown in Fig. S1. Protein preparations were never frozen and after dialysis they were kept not longer than 7 days at 4 °C in PBS pH7.2. Cross-linking was performed with purified Bcl-2 WT recombinant protein (0.37 μg/μl). Sulfosuccinimidyl[perfluoroazidobenzamide]ethyl1,3,dithiopropionate (SFAD, Pierce) (20.5 μg) was used, equal to 3.5 μl of SFAD 10 mM (6 mg/ml) in DMSO. The reaction, in a total volume of 500 μl, was incubated at room temperature for 1 h and subsequently the solution was dialyzed vs. PBS 1× at 4 °C overnight.

The protein conjugated with Sulfo-SFAD was mixed with a solution of the same protein to a double concentration (0.37 μg/μl) and was photoactivated with a UV light source. The samples of conjugated protein and not conjugated protein (control) were run on SDS-polyacrylamide gel.

2.2. Monodimensional and two-dimensional non-reducing/reducing SDS-polyacrylamide gels

Proteins (2 μg) were electrophoresed in reducing and non-reducing conditions in SDS-polyacrylamide gel (12% of acrylamide). For non-reducing condition protein samples were mixed in non-reducing SDS-PAGE (0.25 mM Tris–HCl pH 6.8, 2% (w/v) SDS, 20% (v/v) glycerol, 0.004% (w/v) bromophenol blue) without β-mercaptoethanol and directly loaded into gel.

The reduced and non-reduced protein samples were loaded into the same SDS polyacrylamide gel. Western blot was used to detect the proteins.

A monoclonal antibody anti-polyhistidine, alkaline phosphatase conjugate was used for the immunoblotting (Sigma). The blot was developed using an alkaline phosphatase substrate (BCIP/NBT, Sigma).

For two-dimensional non-reduced/reduced SDS-polyacrylamide gel, proteins were mixed in non-reducing SDS-PAGE sample buffer (0.25 mM Tris–HCl pH 6.8, 2% (w/v) SDS, 20% (v/v) glycerol, 0.004% (w/v) bromophenol blue) and separated by SDS-PAGE on a 10% acrylamide gel. Gel lanes were excised and incubated in buffer containing 50 mM DTT for 10 min and further 10 min in 100 mM IAA before separation through a second SDS-PAGE gel (10%).

2.3. Interaction analysis using surface plasmon resonance (SPR) technology

Interaction analyses were performed using a Biacore T100 (GE Healthcare). Sensor chips, *N*-ethyl-*N*′-hydroxysuccinimide (NHS), *N*-ethyl-*N*′-(3-dimethylaminopropyl) carbodiimmide (EDC) and ethanolamine HC were from GE. Before starting the experiments, 10× PBS stock solution (1× = 137 mM NaCl, 10 mM phosphate, 2.7 mM KCl, pH 7.4) was prepared. Surface of flow cell 4 was activated for 7 min using a mixture of 0.1 M NHS and 0.4 M EDC. For immobilization, the sensor chip was equilibrated with PBS, and then activated by injecting 0.2 M NHS/EDC followed by 5–10 μg injection of appropriate ligand in 10 mM Acetate at the correct pH, according to the scouting procedure (pH 5.0 and 4.0 for Bcl-2 and Bcl-2Δ, respectively). After immobilization, 30 μl of regeneration buffer (4 M guanidine HCl pH 4.0) was injected to remove non covalently bound proteins. An initial series of buffer blanks was injected first to equilibrate fully the system. Finally, analyte was injected from lowest to highest concentrations using two blank injections and one concentration in duplicate. Used analyte concentrations are here following and each individual sensogram was independently recorded (range 0.25–3.5 μM). All analyses were performed at 37 °C, and for studying protein–protein interactions, kinetic data were obtained by diluting the samples in the running buffer PBS supplemented with P20 (0.05%). The surface was regenerated after each injection with 10 μl/min of regeneration buffer.

2.4. Structural analysis of Bcl-2 molecular model

The quality of the resulting Bcl-2 trimeric complex was assessed using PROCHECK v.3.5 [14] and HOPPscore structure evaluator [15] (HOPPscore v1.0 Beta; http://hoppscore.lbl.gov/) softwares and by comparing the results with those obtained for the human Bcl-2 X-ray structure (PDB code: 1GJH). Structural comparison with i) docking starting structure, ii) human Bcl-2 X-ray structure, and iii) Bcl-xL X-ray structures was performed using the Biopolymer and Homology modules of Insight 2005 (Accelrys, San Diego). RMS values on all Cα were calculated.

Dihedral angles and secondary structure of Bcl-2 trimeric model were compared to human Bcl-2 X-ray structure (PDB code: 1GJH) using Prostat/Residue_Dihedral and Prostat/SecondaryClassify (Homology module). Bcl-2 monomers of the trimeric complex were

superimposed on experimentally determined structures of Bcl-2 and Bcl-xL taking into account alpha carbons of structural conserved regions.

The experimentally determined structures of i) the pore-forming domain of colicin A (PDB code: 1COL); ii) KcsA channel of Streptomyces lividans (PDB code: 3EFF); iii) NaK channel of Bacillus cereus (PDB code: 3E8F) and iv) aquaporin of Pichia pastoris (PDB code: 2W1P) were downloaded from the Protein Data Bank (PDB; http://www.rcsb.org/pdb/), and compared to the obtained Bcl-2 trimeric complex using the homology module of Insight 2005 (Accelrys, San Diego).

Sequence alignments were performed using Expresso (3DCoffee) server [16] (T-Coffee, version_7.71, http://www.tcoffee.org/).

The complete experimental description of i) modeling of Bcl-2 and its mutants, ii) docking procedure and iii) simulated annealing procedure is in Supplemental Data.

3. Results

3.1. SPR analysis of Bcl-2 multimerization

Bcl-2 family proteins tend to multimerize with other proteins, including other members of the Bcl-2 family. In order to get insights into this process, human Bcl-2 was expressed and purified and the kinetics of multimerization was assessed using surface plasmon resonance technology (Table 1). A representative result is shown in Fig. 1. The obtained sensograms did not fit to a simple 1:1 interaction. The best fit to the experimental data was obtained using the heterogeneous ligand model, meaning that a simple interaction Bcl-2/Bcl-2 leading to a dimer does not occur and that at least two levels of interactions are present, one occurring with high affinity with a stable binding and a K_D value of 2.33 ± 0.52 nM, and another featuring weaker values, corresponding to a K_D value of 811 ± 76 nM (Table 1.). To further analyze this process, Bcl-2 multimerization was followed in reducing and non-reducing conditions. In SDS page analysis in reducing conditions no interactions and only the free monomer were detectable (Fig. 2a). In non-reducing conditions, along with the monomer another major complex was detectable, migrating at a MW approximately correspondent to a complex formed by three Bcl-2 monomers (Fig. 2a). In order to elucidate the nature of the complex forming at lower affinity, the same experiment was repeated in non-reducing conditions after incubation of the Bcl-2 protein with sulpho-SFAD and UV cross-linking (Bcl-2 CL). Using this procedure, the first interaction occurring between Bcl-2 monomers was covalently stabilized. It was only by employing this approach that a complex correspondent to a Bcl-2 dimer was clearly detectable (Fig. 2a). In these conditions, stabilization of the Bcl-2 dimer did not allow the formation of the trimeric structure, which suggests that dimer formation is an intermediate step in the generation of the more stable trimeric structure of Bcl-2. In order to assess the relevance of pH variations in these interactions, the technique of 2D SDS-PAGE reducing/non-reducing was applied. Both complexes, trimeric and dimeric, fell below the diagonal, thereby indicating the involvement of ionizable residues in both interactions (Fig. 2b). To assess the relevance of the loop in generation of dimers and trimers of Bcl-2, the same experiments were repeated with a mutant of Bcl-2 in which the loop domain (aa 35–91) was deleted and replaced with a linker sequence of four alanine residues (Bcl-2Δ), as described by Chang et al. [17]. Interaction analysis was repeated using Bcl-2Δ as analyte and either Bcl-2Δ or Bcl-2 as ligand (Fig. 1). In both cases there was no high-affinity Bcl-2 trimers formation and the obtained K_D value was 715 ± 162 nM or 261 ± 131 nM using as analytes Bcl-2Δ and Bcl-2, respectively (Table 1). This finding suggests that the loop region is required for the formation of high-affinity trimeric Bcl-2 complexes. In keeping with this view, when run in SDS-PAGE in non-reducing conditions, Bcl-2Δ was unable to generate the stable trimeric Bcl-2

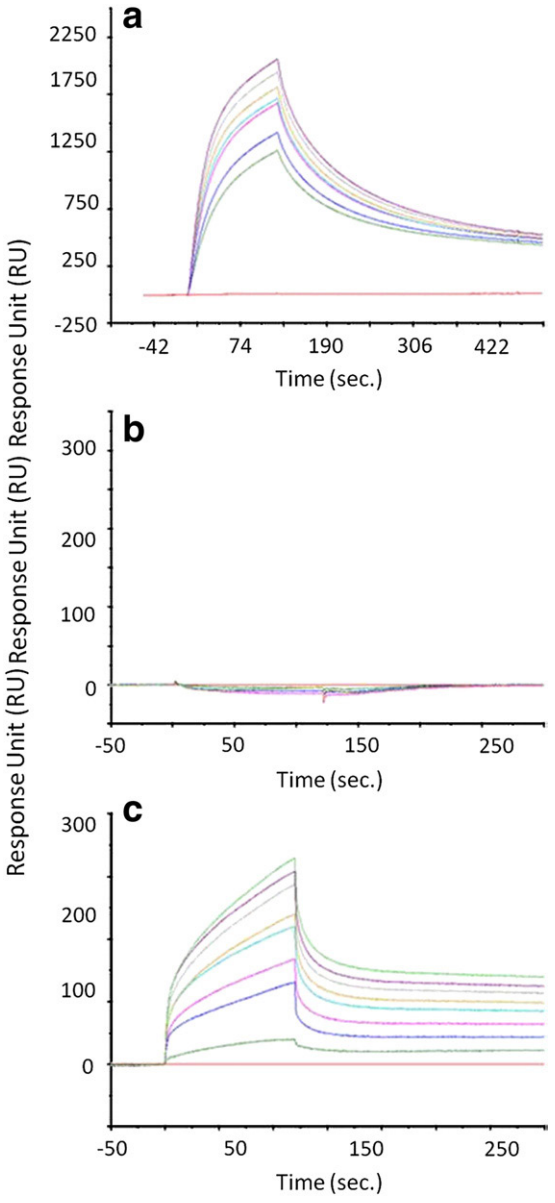

Fig. 1. SPR analysis of the Bcl-2 interactions. Representative sensograms used for the analysis included in Table 1. Bcl-2 was used as analyte, whereas Bcl-2 in native conditions, Bcl-2 in denaturizing and Bcl-2Δ were the analytes for A, B and C, respectively. Each line (sensogram) corresponds to a given concentration of the analyte protein.

Table 1
Main kinetics parameters obtained through SPR analysis using Bcl-2 as ligand and the other proteins as analytes.

	High affinity	Low affinity	No binding
Bcl-2 wt*	Yes	Yes	No
K_D	2.33 ± 0.52 nM	811 ± 76 nM	
Bcl-2 wt (denaturized)	No	No	Yes
Bcl-X_L*	Yes	Yes	No
K_D	6 ± 0.57 nM	2720 ± 200 nM	
Bcl-2Δ**	No	Yes	No
K_D		261 ± 131 nM	
Bcl-2 S70A*	Yes	Yes	No
K_D	0.67 ± 0.09 nM	830 ± 351 nM	
Bcl-2 S70E	No	Yes	No
K_D		984 ± 267 nM	

* Sensograms fitted with the model heterogeneous ligand.
** Sensograms fitted with the 1:1 binding model.

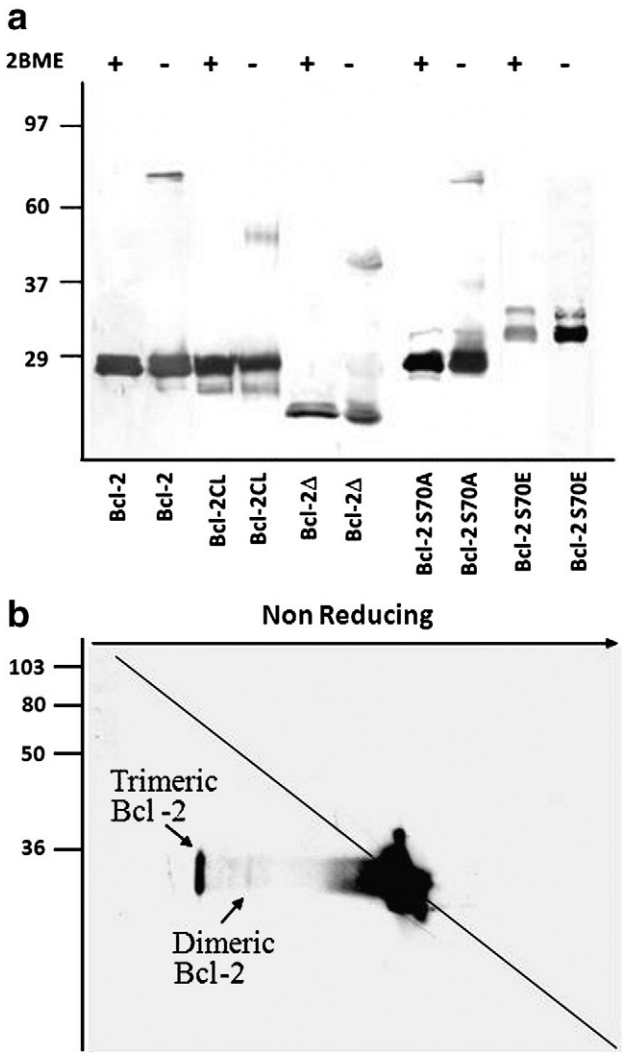

Fig. 2. Immunoblot analysis of the Bcl-2 complexes. (a) Western blot showing Bcl-2 pattern in denaturating (+2BME) and not denaturating conditions (−2BME). A trimeric band was detectable with Bcl-2 and Bcl-2 S70A. Bcl2 CL corresponds to Bcl-2 treated with sulpho-FAD and UV cross-linked. Bcl-2 S70E migrates slightly higher for the extra negative charge. (b) Immunoblotting with anti-Bcl-2 antibody after two-dimensional non-reduced/reduced SDS-PAGE. Proteins lacking disulfide bonds will migrate on the diagonal (gray line) because of the identical mobility in both dimensions. Proteins that contain interchain disulfide-linked complexes will run below the diagonal. Arrows, two major Bcl-2 complexes were detectable corresponding to dimeric and trimeric complexes, respectively.

(Fig. 2a), but only a complex with MW corresponding to that of a dimer.

Conflicting data are present in the literature regarding the role of serine-phosphorylation, but the most recent results tend to support the possibility that phosphorylation at Ser70 inactivates the anti-apoptotic role of Bcl-2 [18]. Also, it has been proposed that the anti-apoptotic function of Bcl-2 is enhanced in a mutant in which Ser is replaced at position 70 with Ala. Due to this mutation, the inactivating phosphorylation at Ser70 cannot occur. In order to correlate the impact of this mutation with the process of multimerization, we repeated the analysis in this S70A Bcl-2 mutant. The low affinity binding site remains unaffected, while high-affinity binding was further enhanced, yielding a K_D value of 0.67 ± 0.9 nM (Table 1). This finding points to the fact that such a mutation does not affect the process of Bcl-2 multimerization. In keeping with these findings, in SDS-PAGE analysis in non-reducing conditions, the formation of the trimeric Bcl-2 complex is easily detectable (Fig. 2a). In contrast, at the same position the mutation S70E was used to simulate the presence of a phosphorylated serine. Again, this mutant served as analyte using Bcl-2S70E itself and Bcl-2 as ligand. Using Bcl-2S70E as ligand and analyte no interactions were detectable, thereby indicating that Bcl-2S70E is not capable of multimerizing with itself. Using Bcl-2S70E as analyte and Bcl-2 as ligand, only the interaction at low affinity was detectable, revealing that it was still able to form complexes with Bcl-2 but not at high affinity (Table 1). In keeping with this hypothesis, when run in SDS-PAGE in non-denaturizing conditions, once again no trimeric structures were detectable in the presence of Bcl-2S70E (Fig. 2a). These results indicate a relationship between the formation of the high-affinity Bcl-2 homo-trimeric complex and the Bcl-2 anti-apoptotic function.

Bcl-X_L exhibits a high structural homology with Bcl-2 and has in common with Bcl-2 its 4 BH domains. The higher divergence in the sequence is present at the level of the disordered loop. To kinetically characterize the interaction Bcl-X_L/Bcl-2, the same analysis was performed using Bcl-2 as ligand and Bcl-X_L as analyte. Similarly to the reaction that occurred with the interaction Bcl-2/Bcl-2, also in this \case two interactions were detectable. The stronger one (K_D 6 ± 0.57 nM) corresponded to the formation of a hetero-dimer of Bcl-X_L/ Bcl-2 with high affinity, the weaker one (K_D 2720 ± 200 nM) to the formation of Bcl-X_L homo-dimers (Table 1). When comparing the results, it is evident that: i) the Bcl-X_L homo-dimer represents a low affinity complex with respect to the Bcl-X_L/Bcl-2 hetero-dimer and ii) a threefold decrease in affinity is present in the interactions Bcl-X_L/Bcl-2 with respect to Bcl-2/Bcl-2.

3.2. Molecular modeling of Bcl-2 homomeric complexes

Molecular models were produced to investigate the ability of Bcl-2 to assume the structure of a homo-trimeric complex, a suggestion which emerged from experimental results. With the aim of exploring this possibility, since all Bcl-2 experimentally determined structures lack the amphipathic loop (aa35-91) and the C-terminal trans-membrane region (aa208-239), our previously developed homology model of human Bcl-2 [19] was integrated through the insertion of the C-terminal helix. The resulting structure was then subjected to flexible docking studies in a complex with other 2 identical monomers (see Materials and methods). The entire structure was included in docking calculations, and distance constraints were applied only to the hydrogen bonds present in those alpha helices that turned out to be highly conserved in secondary structure prediction calculations (http://www.predictprotein.org/) [20], while the rest of the protein was left free of constraints on its movement. Because the docking protocol included a Monte Carlo-based conformational search for "ligand" Bcl-2 in a complex with the 2 other Bcl-2 monomers, the docking procedure was repeated 3 times, each time using a different Bcl-2 monomer as ligand. It is noteworthy that all results converged in the same Bcl-2 homo-trimeric complex structure (Fig. 3) and that, within this trimeric complex, all monomers were structured identically (RMS value on all Cα atoms = 0.38 Å; Fig. 4). These results, together with what was observed in biological assays, indicate a strong tendency for the Bcl-2 loop to form a structure upon interaction with 2 other Bcl-2 loops, thus forming a homo-trimeric complex. The quality of the model was assessed using Procheck (http://www.ebi.ac.uk/thornton-srv/software/PROCHECK/) [14] and Hopp (http://hoppscore.lbl.gov/) [15] and by comparing the results with those obtained for human Bcl-2 X-ray structure (PDB code: 1GJH; Ramachandran plots, Chi1-Chi2 plots, main chain parameters, side chain parameters, and Hopp scores are reported in the Supplemental Data section).

The structure of the docked trimer presents charged loop residues facing the same side of the complex (Fig. 3c and d) and is stabilized by key intra- and intermolecular interactions involving the loop, such as, hydrophobic proline–proline contacts (P39–P40; P44–P46; P57–P59; P59–P71; P71–P75; P88–P90; P90–P91; P53–P78) (Fig. 5a). Furthermore, the loop is structured in several turns, which are stabilized

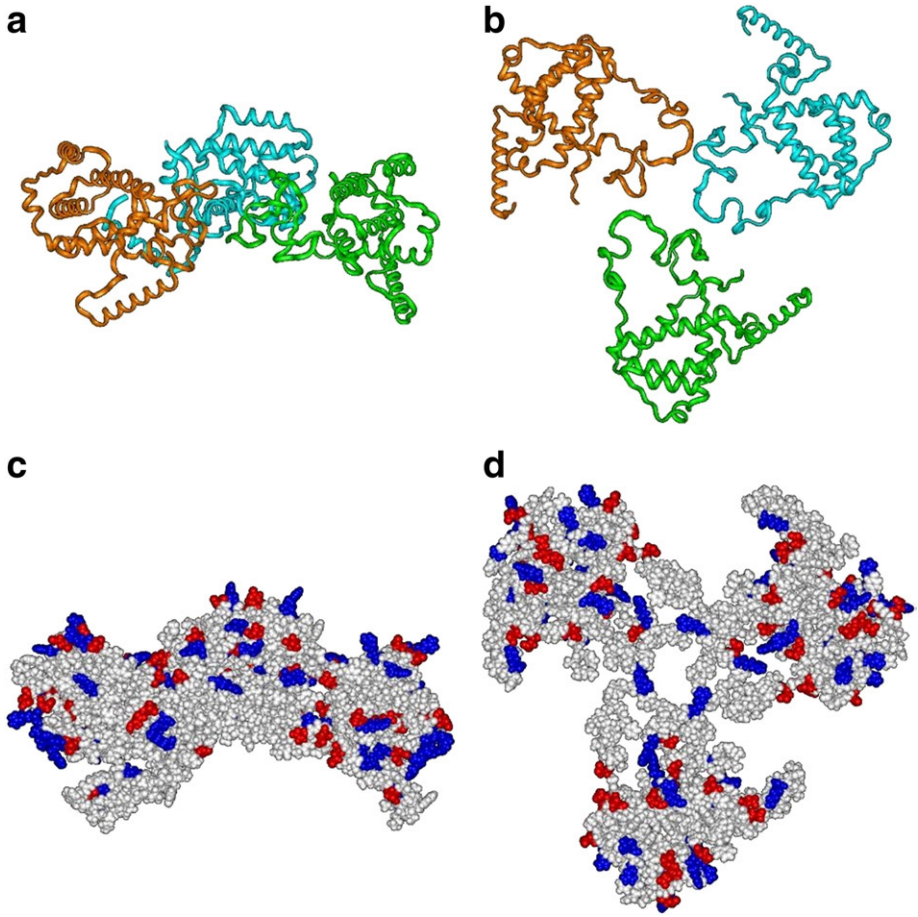

Fig. 3. Overall view of Bcl-2 homo-trimeric complex structure resulting from docking calculations. (a and c) Longitudinal view. (b and d) Transverse view. (a and b) Monomers displayed as ribbons and colored cyan, orange, and green. (c and d) Van der Waals volumes colored by amino acid net charge [neutral: white; negative: red (Asp, Glu); positive: blue (Lys, Arg)]. See also Ramachandran plots, Chi1–Chi2 plots, Main Chain parameters, Side Chain parameters of i) human Bcl-2 X-ray structure (PDB code: 1GJH) and ii) Bcl-2 trimer in Supplemental Data.

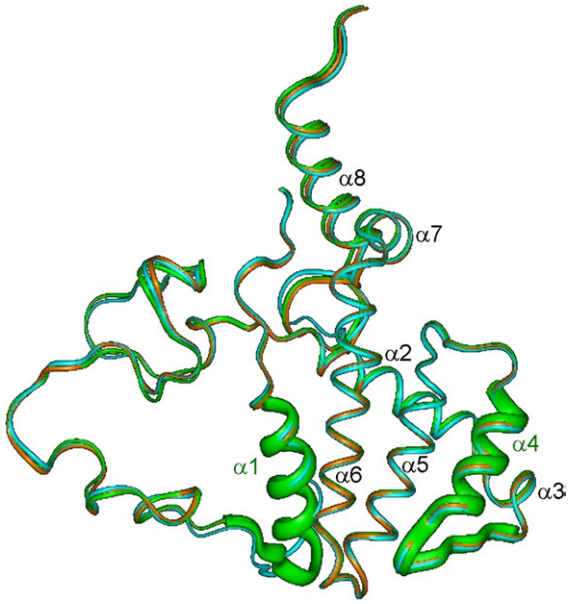

Fig. 4. Superimposition of docked complex monomers taking into account all Cα carbons. Monomers are colored cyan, orange, and green. The 2 P-pore like structures, E13-G33 and Q118-F138, are shown with a thick, green-colored ribbon. See also Fig. S1 and Tables S1 and S2.

either by backbone interactions (A38–G41, G41–A43, I48–S50, P59–A61, S87–V89; Table S2B) or by key hydrogen bonds between amino acid side chains (H55–H58, D64–S70; Fig. 5b and c; Table S2B). Each monomer loop projects an arginine residue (R68) towards the "center" of the complex (Fig. 3d), towards a threonine residue (T56) present on the loop of a partner monomer (Fig. 5c). In contrast, within the same monomer 2 charged loop residues (R63 and D64) face 2 charged residues on α6-helix (E179 and R183; Fig. 5d).

A simulated annealing (SA) procedure was carried out to test the stability of the docked trimer. The docking/SA protocol was also applied to mutants Bcl-2Δ, Bcl-2S70E, and Bcl-2S70A; in addition, in order to simulate reducing conditions used in biological studies, all calculations were repeated at pH values of 5.3 and of 4.0. Consistent with our experimental results, only wild-type Bcl-2 and the S70A mutant (in non-reducing conditions) preserved the homo-trimeric structure at the end of the computational protocol. Indeed, according to our molecular model, i) the replacement of the loop sequence with four Ala residues, ii) the mutation of S70 into a negatively charged glutamate residue (mimicking S70 phosphorylation), as well as iii) the protonation of H55 and H58 residues (occurring at pH 5.3) and iv) aspartate D64 (occurring at pH 4), disrupted key interactions, which, as mentioned above (Fig. 5b and c), stabilized the structure of the complex. Thus our molecular modeling results were in agreement with our experimentally derived data and provide a structural model for the high-affinity Bcl-2 trimeric complex experimentally observed.

Due to the dynamic conditions that existed in docking studies, the resulting structure of Bcl-2 monomers in the trimeric complex turned out to be different from the starting one (RMS value on all Cα

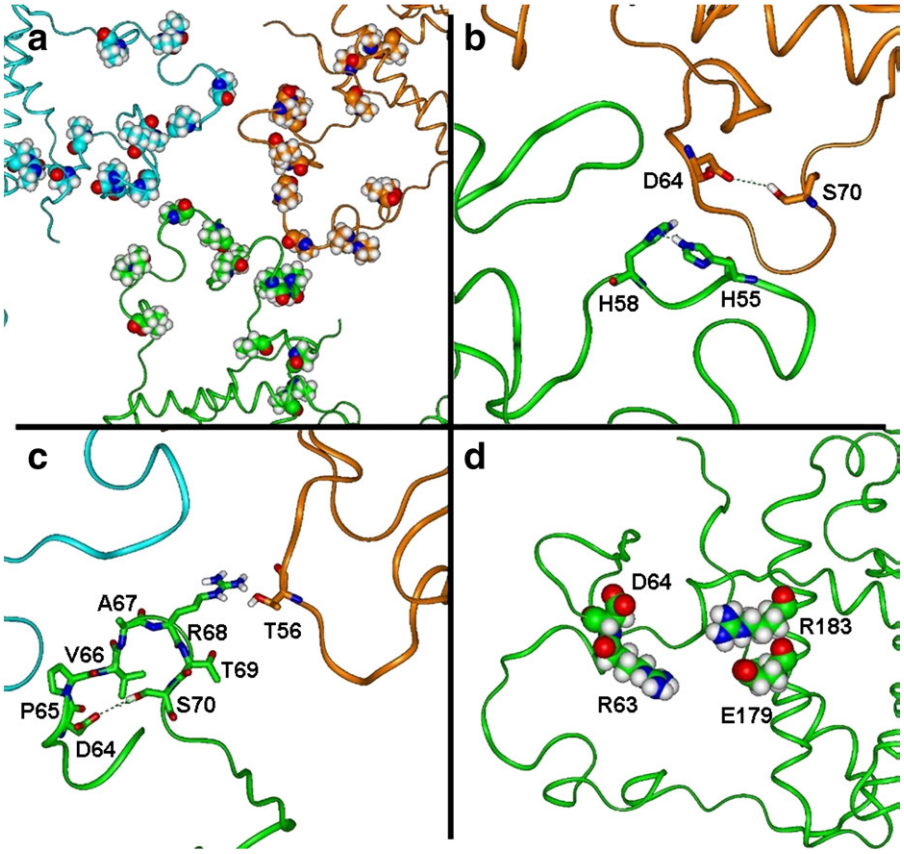

Fig. 5. Overview of major intra- and intermolecular interactions involving the docked trimer loops. Monomers are colored cyan, orange, and green. Amino acids are displayed as van der Waals volumes (a and d) and as sticks (b and c) and colored according to atom type (white for H, blue for N, red for O). Hydrogens are omitted for the sake of clarity, with the exception of those involved in hydrogen bond interactions. Hydrogen bonds are highlighted by green dashed lines. (a) Hydrophobic proline–proline contacts. (b) Intramolecular hydrogen bonds between D64 and S70, as well as H55 and H58. (c) Intermolecular interaction between R68 and T56. (d) R63 and D64 (loop region) facing E179 and R183 (α6-helix).

atoms = 5.9 Å). The conformational changes obtained were analyzed and compared to the X-ray structure of human Bcl-2, as well as to experimentally determined structures of Bcl-XL (Fig. S1). No structural data were available for the Bcl-2 α8 helix and for its long loop, replaced by the Bcl-XL loop in the X-ray structure of human Bcl-2 (1GJH). Major secondary structural changes involved the BH4 domain (D10-F38) and the α3/α4 region (D111-R127) (Table S2). Indeed, our model showed the structural transition of α3 from a 3_{10}-helix (A113-Q118) to a α-turn followed by an uncoiled strand (D111-T122). As a consequence, the region Q118-F138 assumed a P-pore-like structure, i.e., a strand (Q118-T122) and a helix (R127-F138) linked by a hairpin turn to form an antiparallel structure [21]. P-pore regions are characteristic of channels, porins and transporters; accordingly, a structural comparison (Fig. 6) disclosed the similarity between the consensus sequence TxxTxG present in the P-pore of the super-family of voltage-dependent K^+ channels [22] and Bcl-2 motif ^{122}TPFTARG^{128}. In addition, the N-terminal region L23-G33 underwent a similar conformational change since: i) L23-R26 β-turn resolved itself into a α-turn (L23-G27) and ii) the following segment (Y28-G33) structure resolved into an uncoiled strand. As a result, another P-pore-like structure ($helix_{(E13-K22)}$-$turn_{(L23-G27)}$-$strand_{(Y28-G33)}$) was formed at the opposite side of the protein (Fig. 4). Interestingly, the two putative P-pore regions are inversely oriented; in particular, Q118-F138 reproduced the aquaporins' orientation while E13-G33 reproduced the voltage-dependent Na^+/K^+ channels' orientation [23]. These results suggest an intriguing relationship between the ability of Bcl-2 to form structures in homo- and hetero-multimeric complexes and its multi-functional, multifaceted role as a membrane channel.

4. Discussion

Bcl-2 plays a prominent role in regulating the function of mitochondria during respiration, as well as in determining the threshold of apoptotic sensitivity. These functions involve processes of multimerization as well as interactions with partner proteins belonging to the family or outside it. The Bcl-2 system is often viewed as a binary one in which Bcl-2 can interact with itself or with other partners, which in turn can enhance or diminish the anti-apoptotic effect. But is this characterization of Bcl-2 as a binary system correct? Some reports support the process of Bcl-2 homodimerization [24,25] while for other studies this is impossible [26] However, this last study was obtained using murine Bcl-2 and functionality of the protein was not checked after removal of the GST-tag. Noteworthy, the investigation of protein interactions in native conditions is difficult and also in our study we noticed that frozen proteins and preparations older than 1 week are not suitable for functional proteomic analysis, since correct folding of the protein is required to make possible protein–protein interactions. Therefore, these differences can explain different outcomes reported in literature. In this investigation we used SPR technology to directly monitor such interactions. Using this approach we discovered that a Bcl-2 1:1 simple model does not fit with the experimental output of a Bcl-2 multimerization. The high-affinity complex is generated only when 3 molecules of Bcl-2 interact and was absent in reducing conditions. The low affinity dimeric complex is likely an intermediate in the process of Bcl-2 multimerization and is stabilized only upon UV-dependent chemical cross-linking. On the basis of these results, molecular models were produced in order to investigate the ability of Bcl-2 to form a trimeric complex. The models we obtained revealed a strong propensity

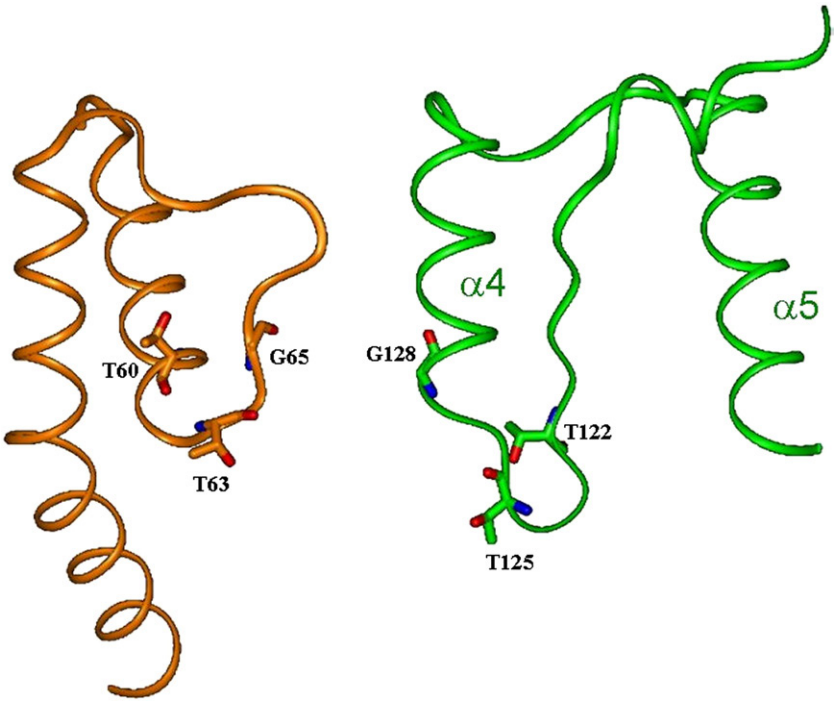

Fig. 6. Comparison between the P-pore region of voltage-dependent Na/K and Bcl-2 docked monomer. Left: P-pore region of the voltage-dependent Na/K channel (PDB Code: 3E8F). Right: Q118-F138 P-pore-like structure of Bcl-2 docked monomer. Conserved amino acids in the consensus sequence TxxTxG of the Na/K channel and in the Bcl-2 motif ^{122}TPFTARG^{128} are evidenced.

of the Bcl-2 loop to form a trimeric structure upon interaction with 2 other Bcl-2 loops, identifying key intra- and intermolecular interactions for the stabilization of the complex. A major advantage of the SPR technology is that several conditions could be investigated simultaneously. Employing this advantage, using selected mutation we gleaned additional insights of the key regions that, according to the model, are involved in the process of multimerization. In the Bcl-2 mutant in whom the entire loop was removed, the protein is unable to form a stable trimeric complex. Since this mutant is functionally unable to protect itself from cell death, this suggests that the formation of the stable trimeric complex through the N-terminal loop is related to the anti-apoptotic function of Bcl-2. In support of this hypothesis, the proteolytic cleavage of the Bcl-2 loop by caspase-3 converts it from an anti-apoptotic to a pro-apoptotic protein [4]. Moreover, the mutant S70A still forms the stable trimeric complex, while the opposite effect is obtained with the mutation S70E. This mutation mimics Serine 70 phosphorylation and was associated with the inhibition of multimer formation. According to our molecular model, the formation of a charge-assisted hydrogen bond between the side chains of S70 and D64 strongly contributes to the stabilization of the trimeric complex (Fig. 5b and c). The replacement of the S70 side chain with a negatively charged group, as occurs in phosphorylation and in the S70E mutant, produces, in contrast, a strong electrostatic repulsion to the D64 side chain, causing the disruption of the entire complex. In fact, Bcl-2S70E cannot bind to itself and interacts with Bcl-2 only by forming dimers at low affinity. Supporting this view, our findings are in line with the literature which reports that this mutation abrogates the anti-apoptotic function of Bcl-2. On the other hand, in reducing conditions only the Bcl-2 monomer is observed. Although the disruption of putative trimer intermolecular disulfide bridges cannot be ruled out, only one cysteine (C229 on the C-terminal helix) per monomer is accessible for disulfide bridge formation, since C158 is buried inside the protein. Moreover, our molecular simulation indicated that in reducing conditions the protonation of loop residues, such as H55, H58, and D64, prevents the formation of key hydrogen bond interactions which stabilized the structure of the trimer, thus avoiding its formation. The crucial role played by the loop in trimer structure and the relation between trimer formation and Bcl-2 anti-apoptotic function, are also consistent with the pro-apoptotic effect induced by non Bcl-2 proteins and small molecules, such as Nur77 and paclitaxel [9,19]. Indeed, the binding of Nur77 and paclitaxel to Bcl-2 loop is not compatible with its structure in the molecular model of the trimer, where it is engaged in key intermolecular interactions; by consequence the binding of paclitaxel and Nur77 to Bcl-2 appears to be alternative of trimer formation.

Concerning interactions with other members of the Bcl-2 family, we investigated the ability of Bcl-X_L to form complexes with Bcl-2. The interaction of Bcl-2 and Bcl-X_L led to the formation of a hetero-dimeric complex. This means that multifamily complexes can also be generated. However, Bcl-X_L/Bcl-2 complex showed a threefold decreased K_D value as compared to the homo-dimeric Bcl-2 complex.

Bcl-2 homo- and hetero-multimerization is also related to its ability to form different channel-like structures. Elegant electrophysiological studies have demonstrated that the current conducted by the ion channels formed by Bcl-2 can be explained by taking into account at least two type of channels, one at low conductance and another with higher conductance [27].The ion channel forming properties of Bcl-2 have been associated with its structural homology to colicins and diphtheria toxin and are likely to play a role in regulating the permeability of mitochondria, particularly the entry of Ca^{++} as also observed in endoplasmatic reticulum [28]. A conformational change is observed in the X-ray structure of the Bcl-X_L dimer, suggesting that an ion channel involving helices α5 and α6 can be formed if more monomers interact [29]. Consistent with the ion channel-forming properties of Bcl-2, conformational changes observed in our Bcl-2 trimeric model include the formation of two P-pore-like structures. The two putative P-pore structures are inversely oriented and are placed at opposite faces of the protein, backed against helices α5 and α6 (Fig. 4). One is located at the N-terminal, just before the loop, and involves the α1 helix (BH4 domain); the other is found in the α3/α4 region and shares the consensus sequence of the selectivity filter for the super-family of voltage-gated K^+ channels (Fig. 6). This latter is part of an hydrophobic groove on the surface of the protein which

represents the interaction site for the pro-apoptotic member of the Bcl-2 family, such as Bak and Bad [30] and several experimental molecular structures of Bcl-XL in complex with BH3 peptides are actually available [31]. In the molecular model of the trimer this hydrophobic groove is still accessible for the putative binding of a partner protein; nevertheless, the P-pore like structure should undergo a conformational change in order to allow the interaction with a BH3 peptide.

In summary, our results support the notion that the Bcl-2 anti-apoptotic function is associated with its ability to integrate itself into the structure of a high-affinity tri-molecular complex through the long N-terminal loop which can modulate the formation of ion channels. If such ion channels play a prominent role in the function of Bcl-2, then the current prevailing view of Bcl-2 as a simple dimeric model seems incomplete.

Acknowledgments

This work was partially supported by a grant coming from Fondazione Banco di Napoli.

Appendix A. Supplementary data

Supplementary data to this article can be found online at doi:10.1016/j.bbamcr.2011.02.006.

References

[1] J.M. Adams, S. Cory, The Bcl-2 protein family: arbiters of cell survival, Science 281 (1998) 1322–1326.
[2] J.C. Reed, Mechanisms of apoptosis, Am. J. Pathol. 157 (2000) 1415–1430.
[3] K. Wang, X.M. Yin, D.T. Chao, C.L. Milliman, S.J. Korsmeyer, BID: a novel BH3 domain-only death agonist, Genes Dev. 10 (1996) 2859–2869.
[4] E.H. Cheng, D.G. Kirsch, R.J. Clem, R. Ravi, M.B. Kastan, A. Bedi, K. Ueno, J.M. Hardwick, Conversion of Bcl-2 to a Bax-like death effector by caspases, Science 278 (1997) 1966–1968.
[5] N. Fujita, T. Tsuruo, Involvement of Bcl-2 cleavage in the acceleration of VP-16-induced U937 cell apoptosis, Biochem. Biophys. Res. Commun. 246 (1998) 484–488.
[6] B. Fadeel, Z. Hassan, E. Hellström-Lindberg, J.I. Henter, S. Orrenius, B. Zhivotovsky, Cleavage of Bcl-2 is an early event in chemotherapy-induced apoptosis of human myeloid leukemia cells, Leucemia 13 (1999) 719–728.
[7] B. Del Bello, M.A. Valentini, F. Zunino, M. Comporti, E. Maellaro, Cleavage of Bcl-2 in oxidant- and cisplatin-induced apoptosis of human melanoma cells, Oncogene 20 (2001) 4591–4595.
[8] C. Ferlini, G. Raspaglio, S. Mozzetti, M. Distefano, F. Filippetti, E. Martinelli, G. Ferrandina, D. Gallo, F.O. Ranelletti, G. Scambia, Bcl-2 down-regulation is a novel mechanism of paclitaxel resistance, Mol. Pharmacol. 64 (2003) 51–58.
[9] B. Lin, S.K. Kolluri, F. Lin, W. Liu, Y.H. Han, X. Cao, M.I. Dawson, J.C. Reed, X.K. Zhang, Conversion of Bcl-2 from protector to killer by interaction with nuclear orphan receptor Nur77/TR3, Cell 116 (2004) 527–540.
[10] S.J. Korsmeyer, X.M. Yin, Z.N. Oltvai, D.J. Veis-Novack, G.P. Linette, Reactive oxygen species and the regulation of cell death by the Bcl-2 gene family, Biochim. Biophys. Acta 1271 (1995) 63–66.
[11] A.J. Kowaltowski, R.G. Fenton, G. Fiskum, Bcl-2 family proteins regulate mitochondrial reactive oxygen production and protect against oxidative stress, Free Radic. Biol. Med. 37 (2004) 1845–1853.
[12] K. Imahashi, M.D. Schneider, C. Steenbergen, E. Murphy, Transgenic expression of Bcl-2 modulates energy metabolism, prevents cytosolic acidification during ischemia, and reduces ischemia/reperfusion injury, Circ. Res. 95 (2004) 734–741.
[13] S.L. Schendel, Z. Xie, M.O. Montal, S. Matsuyama, M. Montal, J.C. Reed, Channel formation by antiapoptotic protein Bcl-2, Proc. Natl Acad. Sci. USA 94 (1997) 5113–5118.
[14] R.A. Laskowski, M.W. MacArthur, D.S. Moss, J.M. Thornton, PROCHECK: a program to check the stereochemical quality of protein structures, J. Appl. Cryst. 26 (1993) 283–291.
[15] G.E. Sims, S.H. Kim, A method for evaluating the structural quality of protein models by using higher-order φ–ψ pairs scoring, Proc. Natl Acad. Sci. USA 103 (2006) 4428–4432.
[16] F. Armougom, S. Moretti, O. Poirot, S. Audic, P. Dumas, B. Schaeli, V. Keduas, C. Notredame, Expresso: automatic incorporation of structural information in multiple sequence alignments using 3D-Coffee, Nucleic Acids Res. 34 (2006) W604–W608, (Web Server issue).
[17] B.S. Chang, A.J. Minn, S.W. Muchmore, S.W. Fesik, C.B. Thompson, Identification of a novel regulatory domain in Bcl-X(L) and Bcl-2, EMBO J. 16 (1997) 968–977.
[18] A. Basu, G. DuBois, S. Haldar, Posttranslational modifications of Bcl2 family members–a potential therapeutic target for human malignancy, Front. Biosci. 11 (2006) 1508–1521.
[19] C. Ferlini, L. Cicchillitti, G. Raspaglio, S. Bartollino, S. Cimitan, C. Bertucci, S. Mozzetti, D. Gallo, M. Persico, C. Fattorusso, G. Campiani, G. Scambia, Paclitaxel directly binds to Bcl-2 and functionally mimics activity of Nur77, Cancer Res. 69 (2009) 6906–6914.
[20] B. Rost, G. Yachdav, J. Liu, The PredictProtein server, Nucleic Acids Res. 32 (2004) W321–W326, (Web Server issue).
[21] D.B. Tikhonov, B.S. Zhorov, Modeling P-loops domain of sodium channel: homology with potassium channels and interaction with ligands, Biophys. J. 88 (2005) 184–197.
[22] R.T. Shealy, A.D. Murphy, R. Ramarathnam, E. Jakobsson, S. Subramaniam, Sequence-function analysis of the K+-selective family of ion channels using a comprehensive alignment and the KcsA channel structure, Biophys. J. 84 (2003) 2929–2942.
[23] G. Fischer, U. Kosinska-Eriksson, C. Aponte-Santamaría, M. Palmgren, C. Geijer, K. Hedfalk, S. Hohmann, B.L. de Groot, R. Neutze, K. Lindkvist-Petersson, Crystal structure of a yeast aquaporin at 1.15 angstrom reveals a novel gating mechanism, PLoS Biol. 7 (2009) e1000130.
[24] M. Hanada, C. Aimé-Sempé, T. Sato, J.C. Reed, Structure-function analysis of bcl-2 protein: identification of conserved domains important for homodimerization with bcl-2 and heterodimerization with bax, J. Biol. Chem. 270 (1995) 11962–11969.
[25] Z. Zhang, S.M. Lapolla, M.G. Annis, M. Truscott, G.J. Roberts, Y. Miao, Y. Shao, C. Tan, J. Peng, A.E. Johnson, X.C. Zhang, D.W. Andrews, J. Lin, Bcl-2 homodimerization involves two distinct binding surfaces, a topographic arrangement that provides an effective mechanism for bcl-2 to capture activated bax, J. Biol. Chem. 279 (2004) 43920–43928.
[26] S. Conus, T. Kaufmann, I. Fellay, I. Otter, T. Rossé, C. Borner, Bcl-2 is a monomeric protein: prevention of homodimerization by structural constraints, EMBO J. 19 (2000) 1534–1544.
[27] A.J. Minn, P. Vélez, S.L. Schendel, H. Liang, S.W. Muchmore, S.W. Fesik, M. Fill, C.B. Thompson, Bcl-x(L) forms an ion channel in synthetic lipid membranes, Nature 385 (1997) 353–357.
[28] F. Vanden Abeele, R. Skryma, Y. Shuba, F. Van Coppenolle, C. Slomianny, M. Roudbaraki, B. Mauroy, F. Wuytack, N.N. Prevarskaya, Bcl-2-dependent modulation of Ca(2+) homeostasis and store-operated channels in prostate cancer cells, Cancer Cell 1 (2002) 169–179.
[29] J.W. O'Neill, M.K. Manion, B. Maguire, D.M. Hockenbery, BCL-XL dimerization by three-dimensional domain swapping, J. Mol. Biol. 356 (2006) 367–381.
[30] A.M. Petros, E.T. Olejniczak, S.W. Fesik, Structural biology of the Bcl-2 family of proteins, Biochim. Biophys. Acta 1644 (2004) 83–94.
[31] a) M. Sattler, H. Liang, D. Nettesheim, R.P. Meadows, J.E. Harlan, M. Eberstadt, H.S. Yoon, S.B. Shuker, B.S. Chang, A.J. Minn, C.B. Thompson, S.W. Fesik. Structure of Bcl-xL–Bak peptide complex: recognition between regulators of apoptosis. Science 275 (1997) 983–986; b) A.M. Petros, D.G.Nettesheim, Y.Wang, E.T. Olejniczak, R.P. Meadows, J.Mack, K. Swift, E.D. Matayoshi, H. Zhang, C.B. Thompson, S.W. Fesik. Rationale for Bcl-xL/Bad peptide complex formation from structure, mutagenesis, and biophysical studies. Protein Sci. 9 (2000) 2528–2534; c) X. Liu, S. Dai, Y. Zhu, P. Marrack, J.W. Kappler. The structure of a Bcl-xL/Bim fragment complex: implications for Bim function. Immunity 19 (2003) 341–352.